Tellus (1991), *43AB*, 16–26

Does low-frequency atmospheric variability exhibit regime-like behavior?

By JOHN M. WALLACE and XINHUA CHENG, *Department of Atmospheric Sciences, University of Washington, Seattle, WA 98195, USA*, and DEZHENG SUN, *Center for Earth and Planetary Physics, Massachusetts Institute of Technology, Cambridge, MA 02139, USA*

(Manuscript received 12 July 1990; in final form 21 November 1990)

ABSTRACT

If the general circulation exhibits nonlinear, regime-like behavior, it should be reflected in the frequency distributions of the state of the atmospheric in phase space either in the form of bi- (or multi-) modality or skewness. In order to determine whether the Northern Hemisphere winter circulation exhibits these characteristics, we examine frequency distributions of (1) the inner product or spatial covariance, (2) the (spatial) "anomaly correlation", and (3) the root mean squared difference or "distance" between each map and each other map in phase space. Our distributions are based on a sample of 702 10-day lowpass filtered, hemispheric 500 mb height anomaly maps (18 maps at 5-day intervals for the equivalent of 39 winter seasons). Excluding pairs of maps from the same winter season, the sample size for the distributions is 240,156. All the frequency distributions of (1) and (2) for the hemispheric maps exhibit a close fit to the corresponding randomly generated distributions based on 20 spatial degrees of freedom. There is no evidence of bimodality. However, the numbers of large positive spatial covariances and anomaly correlations greatly exceed the numbers of their counterparts in the negative tails of the frequency distributions (i.e., "analogues" outnumber "antilogues" of comparable quality). Using a simple form of cluster analysis we show that three rather distinctive blocking patterns account for a disproportionate share of the largest positive values in the frequency distributions. The asymmetries in our frequency distributions may be a reflection of regime-like behavior, but it is also conceivable that they could be the signature of more subtle forms of nonlinearity in the low frequency dynamics.

1. Introduction

The observational meteorologist is confronted with two radically different ways of conceptualizing the low-frequency atmospheric variability in the historical record. The two paradigms relate to the frequency distribution of the instantaneous state of the hemispheric circulation, as viewed in a multi-dimensional "phase space" whose coordinates might be defined as the expansion coefficients of the leading eigenvectors or spherical harmonic coefficients of the 500 mb height field or other indices representing dynamically important quantities. Synoptic charts that closely resemble one another correspond to neighboring points in this phase space. Because of the time continuity inherent in the atmospheric circulation, "state points" that are arbitrarily close together in time are also arbitrarily close together in phase space. Neighboring points may also be laid down in the historical record when the circulation revisits the same region of phase space. We will refer to the latter as recurrent patterns or "analogues."

The "linear paradigm" asserts that the neighborhood of the state point corresponding to the climatological mean circulation should be the most frequently visited region of phase space (i.e., it should correspond to the mode in the frequency distribution of the expansion coefficient of each of the EOF's or spherical harmonics that defines the multi-dimensional phase space). Hence, it is quite natural to view the climatological mean state as the origin in phase space. Departures from the mean should be normally distributed in each dimension so that the cloud of points in phase space thins out monotonically with distance from

the origin in all directions at the same rate. Temporal expansion coefficients of any eigenvectors (or indices preferred structures that might be present, such as the "PNA pattern") should also exhibit a zero mean and a normal distribution in the time domain, so that for synoptic situations characterized by large amplitudes of these anomaly patterns, *antilogues* (a term used by Van den Dool (1987) to denote a situation in which the anomaly pattern on one synoptic chart is analogous to the anomaly pattern of opposing sign on the other) should be just as common as analogues.

The non-linear paradigm views the climatological mean as an arbitrary mathematical construct which need not bear any relation to the most frequently observed state(s) of the atmosphere. It predicts that indices of spatial patterns may exhibit highly skewed or even bi- (or multi-) modal frequency distributions. In relatively simple dynamical systems the modes in such distributions can sometimes be identified with "attractor basins" in mutli-dimensional phase space which correspond to weather or climate *regimes* (Lorenz, 1963; Mo and Ghil, 1988). In more complex systems, structure (i.e., departures from normality) in the frequency distributions may not be as easy to interpret, but it is of no less importance as evidence of nonlinear behavior.

These two contrasting schools of thought can be traced back to the pioneering aerological investigations of the 1940s, some of which interpreted the transient variability in terms of linear, wavelike perturbations about the climatological mean basic state, while others emphasized more discrete transitions of the polar vortex between zonal and meridional flow regimes: the so-called "index cycle". The works on blocking by Berggren et al. (1949) and others exhibit a clear recognition of these two alternative interpretations. With the decline of interest in the index cycle as a long-range forecasting tool in the 1950s, the linear paradigm prevailed virtually unchallenged for several decades. However, interest in nonlinear interpretations of low frequency variability has revived markedly within the past few years, partially in response to advances in the theory of nonlinear systems (for a recent review, see Ghil, 1987) and partially as a result of provocative observational evidence put forth by Charney et al. (1981), Benzi et al. (1986), Sutera (1986), Hansen and Sutera (1986), and Hansen (1986), Molteni et al. (1988, 1990) concerning the bi-modal frequency distribution of certain prescribed general circulation indices.

The following two examples may be helpful in illustrating the range of possible ways in which nonlinear, regime-like behavior might be manifested in atmospheric general circulation statistics, and in setting the stage for the presentation of our results. In the first example, let us suppose that phase space is dominated by two equally distinct equilibrium states whose attractor basins are visited with roughly comparable frequency. In this case, the climatological mean state must lie roughly halfway between the two equilibria and their respective attractor basins in phase space, so that pairs of anomaly maps corresponding to points that lie in the same attractor basin will tend to be positively correlated (in the space domain) with one another, while pairs of maps corresponding to points in different basins will tend to be negatively correlated. If the density of points is substantially larger within the attractor basins than in between them, the frequency distribution of correlation coefficients between pairs of anomaly maps is likely to exhibit a bi-modal distribution, where the positive mode is associated with spatial covariances or correlations between pairs of maps corresponding to points located in the same basin and the negative mode with pairs of maps corresponding to points in the two different basins.

In the second example, let us suppose that the two attractor basins occupy similar volumes of phase space but that one of them is visited much more frequently than the other. As in the previous example, the climatological mean state should lie between the centroids of the points in phase space associated with the two equilibrium states, but in this case it should lie much closer to the centroid of the more frequently visited basin, so as to be virtually surrounded by the points identified with that state. Anomaly maps corresponding to points that lie within the less frequently visited basin, which is relatively far from the origin, should exhibit relatively strong, positive spatial covariances and correlations with one another, but they should exhibit only a weak tendency to be negatively correlated with the maps corresponding to points in the other basin, which surround the origin. The maps corresponding to points that lie

within the more frequently visited basin should not exhibit particularly large covariances with one another, since they lie relatively close to the climatological mean state, and therefore have relatively low amplitudes. Nor should they tend to be particularly strongly positively correlated with one another, since they surround the origin. Hence, in the frequency distributions of the spatial covariances or correlations between all possible pairs of anomaly maps, the regime-like behavior characteristic of simple dynamical systems might be manifested in the form of positive skewness rather than distinct bi- or multi-modality.

In the second example, the more frequently visited cloud of points in phase space need not be associated with a single attractor basin: it might equally well correspond to a linear dynamical regime, or to an amorphous cloud of points associated with a multiplicity of regimes that cannot be distinguished from one another, given the limited size of the data set. As long as most of the points in phase space are identified with that cloud, the above arguments should be applicable regardless of the number of more remote (from the origin), less frequently visited attractor basins that might be present.

With these simple examples in mind, we will now examine sample frequency distributions of (1) the inner product or spatial *covariance* between various pairs of anomaly maps, (2) the spatial correlation coefficient between anomaly maps (commonly referred to as the *anomaly correlation*) and (3) the hemispherically averaged root-mean-squared difference or *distance* between pairs of maps in phase space, based on a large number of pairs of 10-day lowpass filtered 500 mb maps. This methodology was first used in a general circulation context by Lorenz (1969); and it was applied in a format very similar to the one that we will use in a more recent study by Gutzler and Shukla (1984), hereafter referred to as GS. It has also been used to document the persistence of weather regimes by Horel (1985).

Our study is based on gridded United States National Meteorological Center operational analyses of 500 mb height for the winter (December, January, February) seasons during the period January 1946 through December 1984, the equivalent of 39 seasons, compared to 14 seasons used by GS. The data were subjected to (1) preliminary quality control and interpolation to remove erroneous grids and fill gaps in the record so as to obtain complete time series at each gridpoint, (2) removal of the climatological mean annual cycle to produce anomaly time series, (3) low-pass filtering in the time domain to remove fluctuations with periods shorter than about 10 days, and (4) transformation to a 445-point half-resolution grid to reduce the amount of computations required in the subsequent analysis. These procedures are described in Kushnir and Wallace (1989). From the resulting time series, we selected maps at 5-day intervals (December 2, 7, 12, ...); a total of 702 map times (39 seasons at 18 map times). The dates are identical to those for which pentad-mean charts are displayed in the World Meteorological Organization (1983) and the actual gridpoint values should be very similar to the ones on those maps, since the filter used in the recent study has a frequency response similar to a 5-day running mean.

2. Relationships between pairs of maps

Following the procedure used in GS, for each pair of maps in this data set we computed what we will refer to as the *covariance*

$$R_{ij} = \{z_i z_j\},$$

the *anomaly correlation*

$$r_{ij} = \{z_i z_j\} / \{z_i^2\}^{1/2} \{z_j^2\}^{1/2},$$

and the root mean squared distance

$$s_{ij} = \{(z_i - z_j)^2\}^{1/2},$$

where z is the 500-mb height anomaly, the indices i and j identify particular maps in the 702 map data set, and the brackets operator $\{\ \}$ represents an average over the 445 approximately evenly spaced gridpoints. Hence R_{ij}, r_{ij} and s_{ij}, are 702×702 element arrays, in which only half the off-diagonal elements need to be computed (since $R_{ij} = R_{ji}$, etc.). Hence, the number of possible pairs of maps is $(702 \times 701)/2 = 246{,}051$. In the calculations of R_{ij} and r_{ij}, the spatial mean of the data set was not removed. (We actually performed the calculations with and without removing the spatial mean and found that it made very little difference in the results). For purposes of normalization, we also computed the time mean of the spatial standard

deviation $\bar{s} = \overline{\{z_i^2\}^{1/2}} = 84.5$ m where the overbar refers to an average over all 702 map times. $\bar{s}$ can also be viewed as the mean distance of the points from the origin in phase space.

In contrast to GS, whose hemispheric averages are based on the 30–70° N latitude belt, our results are based upon the entire hemisphere poleward of 20° N. Since our domain is larger, our correlations should tend to be slightly weaker than those reported in their study.

Pairs of maps with large positive spatial covariances and anomaly correlations and small rms distances may be a reflection of circulation regimes that persists for 5 days or longer, or they may be a reflection of spatial patterns that recur relatively frequently within the historical record. In the present study, we are primarily interested in latter. Therefore, in computing most of the statistics that we will be dispaying, we imposed the restriction that i and j in the above expressions be representative of maps from different winters. With this restriction, the frequency distribution of R_{ij}, r_{ij} and s_{ij} are comprised of $702 \times (39$ winters @ 18 map times$) \times \frac{1}{2} = 240{,}156$ samples. (The number of "other winters" is 39 rather than 38 because the time series of 500 mb height starts 1 January 1946, so that maps for 40 different winter seasons are involved in the calculations.)

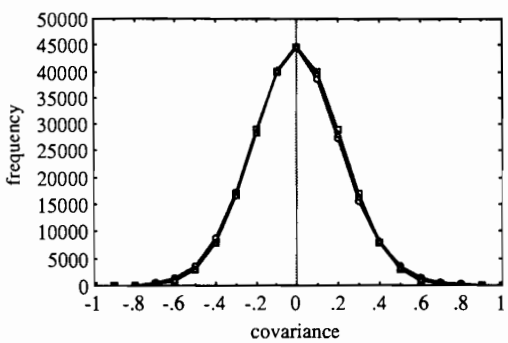

Fig. 1. Frequency distributions of the spatial covariance R_{ij} between all possible pairs of lowpass filtered 500 mb height anomaly maps, scaled by dividing each value by $\bar{s}^2$, the square of the mean spatial standard deviation. Pairs of maps from the same winter are excluded in the distribution (sample size 240,156). The bin width is $0.1\bar{s}^2$ and no smoothing has been performed on the distribution. Circles: observations. Squares: normal distribution with a standard deviation of $1/\sqrt{20}$. Triangles: Monte Carlo simulation for 20 degrees of freedom. Numerical values are tabulated in columns (d), (e), and (f) of Table 1.

Fig. 1 and Table 1 show the frequency distribution of R_{ij}, scaled by dividing each value by $\bar{s}^2$. The figure is based on pairs of maps excluding those from the same winter and the table shows distributions calculated both including and excluding maps for the same winter. Since the sample size is so large, we did not consider it necessary to employ any kind of smoothing of the values in individual bins to make the distribution more

Table 1. *Frequency distribution of the spatial covariance R_{ij} between pairs of 500 mb height maps; (a) observations based on all possible pairs of maps except each map with itself (246,051 pairs); (b)–(c) a normal distribution and results of a Monte Carlo simulation based on 20 degrees of freedom and the same sample size; (d)–(f) as in (a)–(c) but based on all possible pairs of maps except those from the same winter season (240,156 pairs)*

	All possible pairs of maps			Pairs from different winters		
R_{ij}	(a) obs.	(b) normal	(c) rand.	(d) obs.	(e) normal	(f) rand.
−1.3	0	0	0	0	0	0
−1.2	0	0	0	0	0	0
−1.1	0	0	2	0	0	2
−1.0	7	1	5	7	1	5
−0.9	23	7	23	29	7	22
−0.8	127	45	113	124	44	110
−0.7	407	229	409	437	224	400
−0.6	1315	934	1200	1324	911	1161
−0.5	3618	3065	3154	3615	2991	3087
−0.4	8574	8103	8019	8643	7909	7822
−0.3	17358	17259	16985	17165	16846	16578
−0.2	29276	29619	29273	28891	28909	28532
−0.1	40901	40952	41051	39957	39971	40059
0.0	45822	45623	45945	44604	44530	44936
0.1	39717	40952	40739	38631	39971	39754
0.2	27958	29619	28992	27187	28909	28231
0.3	16235	17259	16813	15673	16846	16420
0.4	8294	8103	8238	7922	7909	8064
0.5	3823	3065	3377	3578	2991	3300
0.6	1518	934	1173	1442	911	1146
0.7	635	229	414	556	224	403
0.8	273	45	101	230	44	99
0.9	107	7	20	103	7	20
1.0	40	1	4	27	1	4
1.1	12	0	1	7	0	1
1.2	10	0	0	4	0	0
1.3	1	0	0	0	0	0

representative of the population. From the figure, it is evident that $R_{ij}/\bar{s}^2$ is approximately normally distributed with a standard deviation ~ 0.25. The width of the frequency distribution is an indicator of the equivalent number of spatial degrees of freedom. Consider a random spatial field comprised of N linearly independent (i.e., spatially uncorrelated) gridpoints. For each gridpoint we can construct time series containing the elements a_j, $j = 1, 702$, each of which is drawn from a random normal population with a standard deviation of unity. Each of these N time series, which contributes $1/N$th of the variance $\bar{s}^2$, can be viewed as constituting one spatial degree of freedom of this random field. Since the time series are linearly independent and $\bar{s}^2 = 1$, it follows that

$$\frac{R_{ij}}{\bar{s}^2} = \{a_i a_j\} = \frac{1}{N} \sum_{k=1}^{N} a_{ik} a_{jk}.$$

The distributions of $a_{ik} a_{jk}$ for individual gridpoints are not normally distributed, but it is readily verified that their standard deviation is also equal to unity. As N increases, the population of the average of $a_{ik} a_{jk}$ over N gridpoints approaches a normal distribution, and it narrows approximately in inverse proportion to $\sqrt{N}$. One of the three curves in Fig. 1 corresponds to a Monte Carlo simulation with $N = 22$ (20 degrees of freedom), which we found to produce the best fit to the observations. It is based on 240,156 samples, each of which represents the average of 22 products of random numbers drawn from a normal distribution with a standard deviation of 1. Also plotted in Fig. 1 is the normal distribution corresponding to a standard deviation of $1/\sqrt{20}$. The three curves in the figure are virtually indistinguishable.

Upon inspection of Table 1, which shows the tails of the frequency distributions in more detail, it is evident that there are many more occurrences of strong positive projections, with $R_{ij} > 0.5\bar{s}^2$, than strong negative ones with $R_{ij} < -0.5\bar{s}^2$, and the asymmetry increases as one moves farther out in the tails of the distributions. Such an asymmetry is to be expected in a distribution that includes pairs of maps from the same winter (column (a)), which may be separated in time by as little as 5 days. However it is notable that substantial asymmetry, in the same sense, is also evident in the distribution in which pairs of maps from the same winter are excluded (column (d): it is much larger than in the Monte Carlo simulation, which appears in column (f) of the Table. (H. van den Dool (1989, personal communication) has noticed a similar asymmetry in his search for analogous and antilogous for use in statistical weather prediction: his anomaly correlations are based on circular regions roughly 2000 km in diameter.)

For the observed frequency distribution as a whole (excluding pairs of maps for the same winter), negative covariances outnumber positive ones by 51.2/48.8 %. It is readily verified that the summation of $R_{ij}/\bar{s}^2$ over all pairs of maps, including those from the same winter and each map with itself, must be identically equal to zero. When just the covariances of individual maps with themselves are withheld from the distribution, as in the first column of Table 1, the mean drops to -0.00083, and when all covariances between pairs of maps that fall within the same winter season are withheld, as in the fourth column of Table 1, it drops to -0.0037. Van den Dool (1987) has pointed out this bias toward negative projections in the context of the cross validation of statistical prediction schemes. The asymmetries in the observed frequency distribution are reflected in its moment coefficient of skewness ($+0.095$) which, though barely perceptible in Fig. 1, is statistically significant at a very high confidence level. (According to

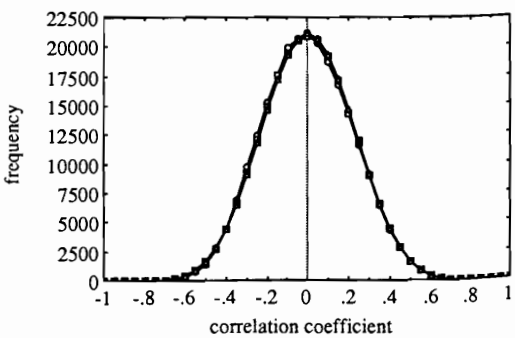

Fig. 2. Frequency distribution of the anomaly correlation r_{ij} between all possible pairs of lowpass filtered 500 mb height anomaly maps, excluding those from the same winter (sample size 240,156). The bin width is 0.05 and no smoothing has been performed on the distribution. Circles: observations. Triangles: Student t distribution for the same sample size with $t = r_{ij}(\sqrt{N-2})/\sqrt{1-r^2}$, where $N-2$, the number of degrees of freedom, is set equal to 20. Squares: results for the Monte Carlo simulation with 20 degrees of freedom.

Brooks and Carruthers (1953), when N, the number of samples, is large, the standard error in the skewness is given by $z = \sqrt{6/N}$. Based on this test, the observed distributions of $R_{ij}/\bar{s}^2$ and r_{ij} both depart from the normal distribution by more than 10 standard errors, which is indicative of confidence levels far in excess of 99.99 %.)

The frequency distribution of r_{ij}, shown in Fig. 2 is qualitatively similar to that of R_{ij}. When compared with the Student t distribution for $t = r\sqrt{N-2}/\sqrt{1-r^2}$, and with a Monte Carlo simulation based on correlation coefficients between sums of products of pairs of number drawn from a normalized, random normal distribution, it also exhibits the closest agreement when 20 is used as the number of degrees of freedom (i.e., with the sum of 22 products in the Monte Carlo simulation). The tails of the same frequency distributions are shown in more detail in Table 2. This time only results for the distribution generated by excluding pairs of maps from the same winter are shown in the Table. The corresponding cumulative frequency distributions shown in the lower rows of the Table were constructed by starting at the tails of the distribution and working inward toward the center.

Table 2. *Positive (+) and negative (−) tails of the frequency distribution of the anomaly correlation r_{ij} between all possible pairs of 500 mb height maps, excluding those from the same winter (sample size 240,156); "obs" denotes observed values; "rand" denotes values from the Monte Carlo simulation; and "t" denotes values calculated from the theoretical Student t distribution; the cumulative frequency distributions are calculated working inward from the tails*

$\lvert r_{ij}\rvert$	0.50	0.55	0.60	0.65	0.70	0.75	0.80	0.85
obs. +	1545	809	388	149	44	6	0	0
obs. −	1378	720	255	69	8	1	0	0
"t"	1605	839	390	156	52	14	3	0
rand. +	1607	828	387	129	46	13	0	1
rand. −	1613	843	383	175	48	14	4	1
Cumulative								
$\lvert r_{ij}\rvert$	0.50	0.55	0.60	0.65	0.70	0.75	0.80	0.85
obs. +	2941	1396	587	199	50	6	0	0
obs. −	2431	1053	333	78	9	1	0	0
"t"	3059	1454	615	225	69	17	3	0
rand. +	3011	1404	576	189	60	14	1	1
rand. −	3081	1468	625	242	67	19	5	1

It is evident from Fig. 2 and the Table 2 that the theoretical distribution fits the Monte Carlo simulation extremely well, even in the tails of the distribution, and that both fit the observed distribution fairly well. It is notable that the asymmetry between the positive and negative tails of the observed frequency distribution is about a factor of five larger than that in the Monte Carlo simulation. The moment coefficient of skewness of the distribution (0.063) is highly significant, but is substantially smaller than the corresponding value for the frequency distribution of R_{ij}. The difference between the two distributions suggests that the analogues in the positive tail of the frequency distribution tend to be characterized by large spatial standard deviations s_i. If this is, in fact, the case we might expect the ensemble mean of $s_i s_j/\bar{s}^2$ for the 240 (0.1 %) pairs of maps with the highest values of r_{ij} to be substantially higher than 1.0. The observed value for the hemispheric maps is 1.18, which is statistically significant at a level well beyond 99.99 %. This result is consistent with the heuristic argument in Section 1.

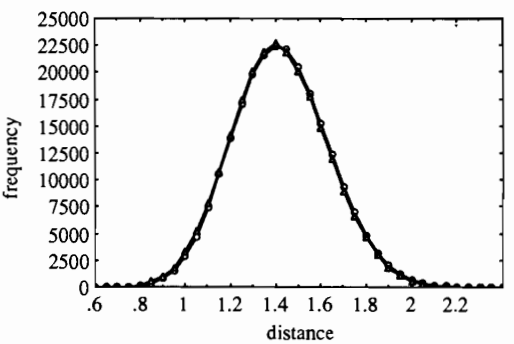

Fig. 3. Frequency distribution of the root mean square difference, averaged over all gridpoints, referred to as the "distance" s_{ij} between all possible pairs of lowpass filtered 500 mb height anomaly maps, excluding those from the same winter (sample size 240,156), scaled by dividing each value by $\bar{s}$, the mean spatial standard deviation about the climatological mean map. The bin width is $0.05\bar{s}$ and no smoothing has been performed on the distribution. Circles: observations. Triangles: Monte Carlo simulation with 20 spatial degrees of freedom.

The corresponding distribution of s_{ij}, scaled by dividing each value by $\bar{s}$, is shown in Fig. 3. For the distribution as a whole, including maps within the same winter and each map with itself, it is readily verified that the mean value of s_{ij} must be identically equal to $\sqrt{2}\,\bar{s}$. The closest "neighbors" in the frequency distribution are on the order of $0.6\bar{s}$ apart and the farthest are about $2.3\bar{s}$ apart. Only a few hundred pairs of maps are separated by less than $0.85\bar{s}$. Hence, consistent with the results of Lorenz and GS, the historical record is far too short to provide really close analogues among hemispheric maps.

3. Cluster analysis

In order to further explore the distribution of hemispheric 500 mb height patterns in phase space, we performed cluster analysis, using the rather simple method proposed by Ward (1963) and discussed in more detail by Wishart (1969), which exploits the distance matrix described in the previous section, where all possible pairs of maps are included in the distribution, except each map with itself. Starting with all 702 maps, the two closest neighbors in that distribution are identified and averaged together to form a new map (i.e., a cluster with two members) which, in subsequent calculations, replaces the two maps from which it was formed. The distances between this new map and all the remaining 700 maps are then computed, and the revised distance matrix is inspected to identify the two closest neighboring maps. These two maps, in turn, are averaged to form a new map, and the procedure was repeated until, after 701 iterations, only a single map remains. Each time two maps are averaged to form a new or enlarged "cluster", they are weighted in accordance with the number of maps that have been averaged together to form them. For example if, on the second iteration, the two-member cluster map merges with another map to form an enlarged cluster, it receives twice as much weight as the other map. It is readily verified that the final "product" of this procedure is the 702 element cluster that constitutes the climatological mean map. We then work backwards from the final step and inspect the two clusters that merged to form the climatological mean map, and trace back to find the two clusters that merged to form them, etc., until we encounter clusters too small to be of interest. A small segment of the resulting "family tree" is shown in Fig. 4 and mean maps that correspond to the centroids of three of the more interesting clusters are shown in Fig. 5.

The statistical significance of the clusters derived from this procedure is a rather involved issue that is beyond the scope of this paper. It will suffice to say that (1) the clusters shown in Fig. 5 are quite reproducible in subsets of the data, (2) they are recoverable (though with somewhat reduced amplitude) in a cluster analysis based on the first five principal components of the 500 mb height field and (3) they are remarkably similar to some of the clusters identified by Kimoto (1987, 1989) using a "bump hunting" algorithm that bears little resemblance to Ward's scheme. In the latter study the analysis was based upon direction in phase space (relative to the origin) rather than distances between pairs of maps.

The cluster analyses of Mo and Ghil (1988) and Molteni et al. (1990) did not yield patterns similar to those shown in Fig. 5. In the former the clusters were defined in terms of direction in a seven dimensional phase space. In contrast to Kimoto's studies, in which the phase space was defined in terms of the empirical orthogonal functions of the covariance matrix, Mo and Ghil defined their phase space in terms of the empirical orthogonal functions of the temporal *correlation* matrix. The resulting patterns tend to be of lower amplitude and more wavelike than those obtained by Kimoto and us. When, in response to a suggestion of

72						25
94	**166**				**85**	60
		423	702	279		
122	257				194	64
135						130

Fig. 4. Summary of the results of the last 7 steps in the cluster analysis. The center number (702) represents the final cluster, with 702 members, which corresponds to the climatological mean map. It is flanked by the two clusters (with 423 and 279 members), which merged in the final step of the analysis to form it. Those two cluster, in turn, are connected to the two clusters that merged to form them, etc., to form a schematic "family tree". Maps for the points in phase space that correspond to the centroids of the clusters indicated in boldface type are shown in the Fig. 5.

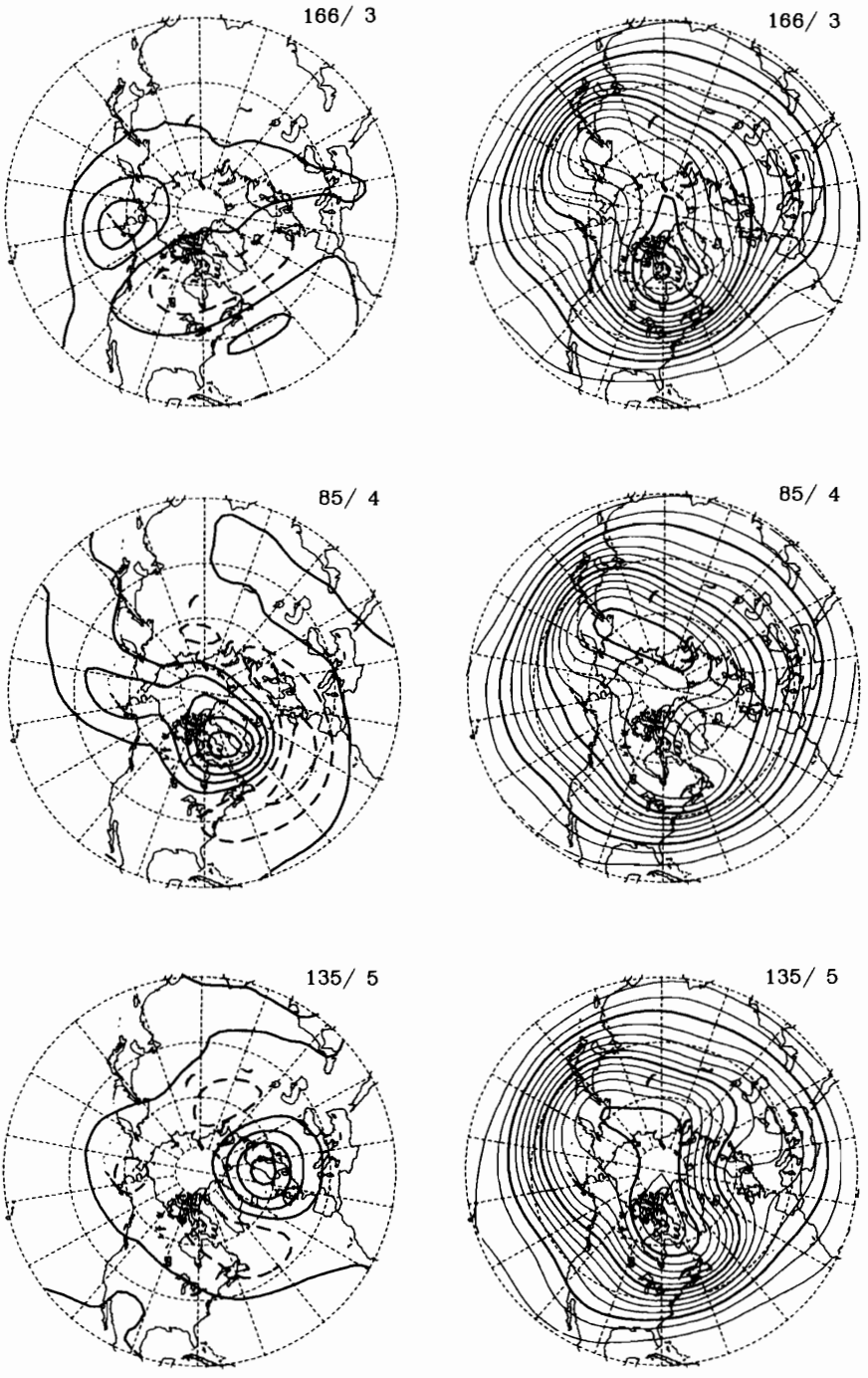

Fig. 5. Left: anomaly maps for the points in phase space that correspond to the centroids of three of the more reproducible clusters depicted in the previous figure. Right: the corresponding composite maps for the total 500 mb height field. Printed at the upper right of the anomaly maps is the number of maps in the cluster.

Kimoto, we repeated our analysis using the correlation matrix in place of the covariance matrix, our patterns became much weaker and more wavelike. The results of Molteni et al. are difficult to compare with the others because they are based on perturbations from the zonal mean basic state, and hence they do not have a zonally symmetric component.

All three patterns in Fig. 5 are characterized by distinctive blocking signatures: i.e., a single prominent region of positive height anomalies along 60° N that corresponds to a well defined ridge in the corresponding composite map. In contrast to the patterns derived from conventional or rotated component analysis, the patterns associated with these clusters tend to be less wavelike; their amplitude tends to be more concentrated in a single "center of action". It is notable that for none of these patterns does there exist a counterpart cluster of opposite polarity, with negative height anomalies as its primary center of action. All three patterns are formed from the merging of "subclusters", some of which exhibit patterns similar to those in Fig. 5 but with substantially larger positive anomalies in the vicinity of their primary "center of action".

We have attempted to crudely quantify, in Table 3, the contribution of these three clusters to the skewness of the frequency distribution of r_{ij}. This table, which is presented in the same format as the previous one, was constructed as follows. We extracted from the 702 maps in the data set, the ones associated with the three clusters shown in Fig. 5; a total of $(85 + 135 + 166) = 386$ maps and we subjected these maps to the analysis described in Section 2, just as if they constituted the entire data set. Pairs of maps from the same winter were not included in the distribution. The results are presented in the rows labeled C in the Table. We then performed a similar analysis upon the remaining $702 - 386 = 316$ maps and printed the results in the rows labeled NC. To make the results comparable, we expressed the frequencies for all rows in units of number of pairs of maps per 100,000. In both the C and NC columns the positive correlations outnumber negative correlations in the tails of the distributions (not shown), but this tendency is clearly much stronger in the subset of the maps (C) associated with blocking.

Table 3. *Positive tails of frequency distributions of the anomaly correlation r_{ij} between pairs of maps drawn from subsets of the data set; C denotes the subset consisting of all the maps in the three clusters shown in Fig. 5 (25481 pairs); NC denotes the subset consisting of all the maps not in those three clusters (48438 pairs); in both distributions, pairs of maps from the same winter are excluded; frequencies are expressed in terms of numbers of pairs of maps per 100,000; the cumulative frequency distributions are calculated working inward from the tails*

$\lvert r_{ij}\rvert$	0.50	0.55	0.60	0.65	0.70	0.75	0.80	0.85
C+	2029	1356	754	349	110	20	0	0
NC+	950	481	215	81	25	2	0	0
Cumulative								
C+	4618	2589	1233	479	130	20	0	0
NC+	1754	804	323	108	27	2	0	0

4. Discussion

The observational evidence of nonlinear "regime like" behavior presented in the previous two sections is rather subtle. In none of the frequency distributions that we examined did we find evidence of outright bimodality analogous to that reported in the studies cited in the Introduction, nor did any of the more prominent spatial patterns that emerged in our cluster analysis strongly resemble those that have been reported in association with bimodality. However, we do see evidence of the skewed frequency distributions that one should expect to prevail in a system that exhibits one (or more) multiple equilibria relatively far removed from the mean state, which is (are) observed only a relatively small fraction of the time. Blocking episodes appear to be responsible for much of the observed skewness. It is interesting to note that skewness is common, not only in the frequency distributions documented in this paper, but also in time series of 500 mb height itself (White, 1980, Nakamura and Wallace, 1991). The strongest positive skewness is, in fact, observed over the northern oceans, in regions noted for blocking.

The existence of skewed frequency distributions does not, in and of itself, constitute definitive proof of the existence of regime-like behavior. For example, in the presence of a zonally varying basic state, pairs of numerical integrations of the barotropic

vorticity equation with identical forcing, but for the sign, exhibit significant differences in shape and amplitude of the resulting finite amplitude perturbations (Simmons et al., 1983). Such asymmetries could produce widespread skewness in the frequency distributions of 500 mb height and other general circulation statistics, even in the absence of well defined regime-like behavior. Nor does the evidence that we have presented preclude the possible existence of more distinct hemispheric circulation regimes such as those reported in the observational studies cited in the Introduction. In the presence of seasonal and interannual variability of the boundary forcing and superposed, slowly propagating planetary waves, such regimes, even if they existed, might not be clearly revealed in the analysis employed in this paper, which relies heavily upon linear correlations. Hence, the question of whether low-frequency atmospheric variability exhibits regime-like behavior may prove very difficult, if not impossible to answer definitively on the basis of observational evidence alone.

The analysis in Section 2 indicates that the number of spatial degrees of freedom in the 10-day lowpass filtered hemispheric maps is of order 20. Van den Dool and Chervin (1986) have made similar estimates based on anomaly correlations between monthly mean maps and found values of 15–20 for the winter months. Such estimates, based on monthly mean maps should be expected to be somewhat smaller than ours because the anomaly patterns tend to be simpler and larger in horizontal scale than those in more lightly lowpass filtered charts (Blackmon et al., 1984; Kushnir and Wallace, 1989).

5. Acknowledgments

The calculations are based on a data set prepared by Yochanan Kushnir. Ward's method of cluster analysis was brought to our attention by Hisashi Nakamura. Discussions with Masahide Kimoto were helpful in clarifying the similarities and differences among the published results of cluster analysis of the Northern Hemisphere wintertime geopotential height field. This work was supported by the Climate Dynamics Program Office in the Atmospheric Sciences Division of the National Science Foundation under Grant Number ATM 8822872.

REFERENCES

Blackmon, M. L., Lee, Y.-H. and Wallace, J. M. 1984. Horizontal structure of 500 mb height fluctuations with long, intermediate and short time scales. *J. Atmos. Sci. 41*, 961–979.

Benzi, R., Malguzzi, P., Speranza, A. and Sutera, A. 1986. The statistical properties of the atmospheric general circulation: observational evidence and a minimal theory of bimodality. *Quart. J. Roy. Meteorol. Soc. 112*, 661–674.

Berggren, R., Bolin, B. and Rossby, C.-G. 1949. An aerological study of zonal motions, its perturbations and breakdown. *Tellus 1, 2*, 14–37.

Brooks, C. E. P. and Carruthers, N. 1953. *Handbook of Statistical Methods in Meteorology*. Her Majesty's Stationary Office, 54–58, 88–94, 112–113, 124–129.

Charney, J. G., Shukla, J. and Mo, K. C. 1981. A comparison of blocking theory with observations. *J. Atmos. Sci. 38*, 762–779.

Ghil, M. 1987. Dynamics, statistics and predictability of planetary flow regimes. In: *Irreversible phenomena and dynamical systems analysis in the geosciences*, (eds. C. Nicolis and G. Nicolis). D. Reidel, Hingham MA, 241–283.

Gutzler, D. S. and Shukla, J. 1984. Analogues in the wintertime 500 mb height field. *J. Atmos. Sci. 41*, 177–189.

Hansen, A. R. 1986. Observational characteristics of atmospheric planetary waves with bimodal frequency distributions. *Anomalous atmospheric flows and Blocking*, (eds. R. Benzi, B. Saltzman and A. Wiin-Nielsen). Advances in Geophysics, 29, Academic Press, 459 pp.

Hansen, A. R. and Sutera, A. 1986. On the probability density distribution of planetary-scale atmospheric wave amplitude. *J. Atmos. Sci. 41*, 3250–3265.

Horel, J. D. 1985. Persistence of the 500 mb height field during the northern winter. *Mon. Wea. Rev. 113*, 2030–2042.

Kimoto, M. 1987. *Analysis of recurrent flow patterns in the Northern Hemisphere winter*. M.S. Thesis, Department of Atmospheric Sciences, University of California at Los Angeles, Los Angeles, CA 90024.

Kimoto, M. 1989. Multiple flow regimes in the Northern Hemisphere winter. Ph.D. Thesis, Department of Atmospheric Sciences, University of California at Los Angeles, Los Angeles, CA 90024.

Kushnir, Y. and Wallace, J. M. 1989. Low-frequency variability in the Northern Hemisphere winter: geographical distribution, structure and time-scale dependence. *J. Atmos. Sci. 46*, 3122–3142.

Lorenz, E. N. 1963. Deterministic nonperiodic flow. *J. Atmos. Sci. 20*, 130–141.

Lorenz, E. N. 1969. Atmospheric predictability as revealed by naturally occurring analogues. *J. Atmos. Sci. 26*, 636–646.

Mo, K. and Ghil, M. 1988. Cluster analysis of multiple planetary flow regimes. *J. Geophys. Res. 93*, 10927–10952.

Molteni, F., Sutera, A. and Tronci, N. 1988. The EOF's of the geopotential eddies at 500 mb in winter and their probability density distributions. *J. Atmos. Sci. 45*, 3063–3080.

Molteni, F., Tibaldi, S. and Palmer, T. N. 1990. Regimes in the wintertime circulation over northern extratropics. I. Observational evidence. *Quart. J. R. Meteorol. Soc. 116*, 31–67.

Nakamura, H. and Wallace, J. M. 1991. On the skewness of low-frequency fluctuations in the tropospheric circulation during the Northern Hemisphere winter. *J. Atmos. Sci. 48*, in press.

Simmons, A. J., Wallace, J. M. and Branstator, G. W. 1983. Barotropic wave propagation and instability, and atmospheric teleconnection patterns. *J. Atmos. Sci. 40*, 1363–1392.

Sutera, A. 1986. Probability density distribution of large-scale atmospheric flows. *Anomalous atmospheric flows and Blocking*, (eds. R. Benzi, B. Saltzman and A. Wiin-Nielsen). Advances in Geophysics, 29, Academic Press, 459 pp.

Van den Dool, H. 1987. A bias in skill in forecasts based on analogues and antilogues. *J. Clim. & Appl. Meteor. 9*, 1278–1281.

Van den Dool, H. and Chervin, R. W. 1986. A comparison of month-to-month persistence of anomalies in a general circulation model and in the earth's atmosphere. *J. Atmos. Sci. 43*, 1454–1466.

Ward, J. 1963. Hierarchical grouping to optimise an objective function. *J. Amer. Statist. Assoc. 58*, 236–244.

White, G. H. 1980. Skewness, kurtosis and extreme values of northern hemisphere geopotential heights. *Mon. Wea. Rev. 108*, 1446–1455.

Wishart, D. 1969. An algorithm for hierarchical classifications. *Biometrics 25*, 165–170.

World Meteorological Organization. 1983. Five-day mean 500 hPa height and mean sea-level pressure fields for the Northern Hemisphere (1946–1977). *Long-range forecasting Research Publications Series 2, vol. 1: Winter*, 191 pp.